plasma

MDPI

Article

Bacterial and Biofilm Inactivation in Tubular Systems Using Surface Dielectric Barrier Discharge with Liquid Electrodes

Oleksandr Galmiz [1,*], Bernard Gitura Kimani [1], Mária Peťková [2], Styliani Roufou [3], Vasilis Valdramidis [3] and Zdenko Machala [1]

[1] Division of Environmental Physics, Faculty of Mathematics, Physics and Informatics, Comenius University in Bratislava, Mlynská Dolina, 842 48 Bratislava, Slovakia; bernard.kimani@fmph.uniba.sk (B.G.K.); zdenko.machala@fmph.uniba.sk (Z.M.)

[2] Department of Genetics, Faculty of Natural Sciences, Comenius University in Bratislava, Mlynská Dolina, 842 48 Bratislava, Slovakia; petkova21@uniba.sk

[3] Laboratory of Food Chemistry, Department of Chemistry, National and Kapodistrian University of Athens, 157 72 Athens, Greece; stylianirouf@chem.uoa.gr (S.R.); vasilis.valdramidis@chem.uoa.gr (V.V.)

* Correspondence: oleksandr.galmiz@uniba.sk

Abstract

Biofilm formation on material surfaces represents a major challenge in many technological and biomedical applications, particularly in confined geometries such as tubes and channels. In this study, the antibacterial performance of a surface dielectric barrier discharge system with liquid electrodes was investigated to develop a plasma-assisted approach for inactivating bacterial biofilms on internal surfaces. The discharge operated along the inner surface of the dielectric tubes as it was gradually filled with water. This configuration created a dynamic plasma–liquid environment in which plasma filaments propagated along the treated surface, while reactive species were produced simultaneously in both the gas and liquid phases. The formation of reactive oxygen and nitrogen species in plasma-treated water was characterized, and its antimicrobial activity was evaluated against planktonic *Escherichia coli* CCM 3954. The effectiveness of both plasma-activated water and direct plasma exposure in inactivating *E. coli* biofilms grown on the inner surfaces of polymer tubes was also investigated. The results demonstrate that the investigated surface dielectric barrier discharge configuration enables simultaneous direct plasma treatment and in situ generation of plasma-activated water. This approach shows promise for plasma-assisted decontamination of tubular materials and confined systems, where conventional disinfection methods may be limited.

Keywords: bacteria; biofilm; *E. coli*; plasma; plasma activated water; polymer

Academic Editor: Dariusz Z. Korzec

Received: 3 August 2026
Revised: 31 August 2026
Accepted: 2 September 2026
Published: 5 September 2026

1. Introduction

Bacterial contamination and biofilm formation on material surfaces pose persistent challenges across a wide range of applications, including medical devices, water distribution systems, food-processing equipment, and industrial pipelines. Once established, biofilms exhibit significantly enhanced resistance to conventional antimicrobial agents due to the presence of a structured extracellular polymeric substance (EPS) matrix that protects embedded microorganisms and limits the penetration of disinfectants. As a result, the development of efficient methods to remove and inactivate biofilms on material surfaces remains an important technological objective.

In recent years, non-thermal atmospheric pressure plasmas have emerged as a promising tool for microbial decontamination and surface sterilization [1–4]. Plasma treatment can be employed to alter the surface characteristics of materials, improving their biocompatibility and functionality. Such modifications can make materials suitable for specific applications where they might not have been useful without plasma treatment. Non-thermal plasma generates a variety of chemically reactive species collectively referred to as reactive oxygen and nitrogen species (RONS), including hydroxyl radicals (•OH), atomic oxygen (O), hydrogen peroxide (H_2O_2), and nitrogen oxides [5,6]. These species can induce oxidative damage to cellular components, disrupt bacterial membranes, and degrade biomolecular structures within microbial cells. In addition to chemical effects, plasma treatment can involve physical mechanisms such as electric fields, charged particles, and UV emission, which may further contribute to microbial inactivation [7,8].

Non-thermal atmospheric pressure plasma generation can be achieved using various discharge configurations, including corona discharge, micro-hollow cathode discharge, dielectric barrier discharge, gliding arc, and plasma jets [9]. The efficiency and composition of the plasma depend on the discharge reactor configuration and operating parameters, such as applied voltage, gas composition, temperature, humidity, and power frequency [10,11].

Two principal approaches are commonly employed in plasma-based antimicrobial applications. In direct plasma treatment, microorganisms are exposed directly to the plasma discharge and to short-lived reactive species generated at the plasma–surface interface. Alternatively, in indirect plasma treatment, plasma-activated water (PAW) can be produced, in which long-lived reactive species accumulate in the liquid and exert antimicrobial effects after plasma exposure. PAW has attracted considerable attention because it can be applied to complex or sensitive surfaces where direct plasma exposure may be impossible or impractical. The antimicrobial activity of PAW is typically attributed to a combination of hydrogen peroxide, nitrogen oxides, and acidification, which together create a chemically reactive environment that inactivates microorganisms.

PAW results from treating water with a plasma discharge and exhibits broad potential in areas like cancer cell targeting, wound care, food preservation, and bacterial inactivation [8,9,12,13]. Due to its multi-target action, PAW minimizes the likelihood of microbial resistance [14,15]. Despite these advantages, PAW's ability to combat biofilms, which are structured communities of bacteria embedded in a self-generated extracellular matrix, remains less explored. Biofilms present substantial challenges in medical and industrial contexts, causing persistent infections and biofouling in water systems and food processing facilities [16–22].

Moreover, the plasma-induced effect also depends on the type of microbial contaminants, their metabolism, and their response mechanisms against stress conditions. Therefore, it is crucial to determine the concentrations of species produced in the plasma gas phase, understand their subsequent transport into water, and quantify the concentrations of reactive species in water. Antibacterial effects are likely not the result of a single reactive species, but rather of a combination of reactive species, determined primarily by discharge properties and gas-mixture composition.

Despite significant progress in this field, most current research on plasma-modified biomaterials uses plasma reactors to treat planar surfaces of small disks or films. However, these reactors are not suitable for modifying the internal surfaces of narrow or tubular structures. Plasma quenching near tube ends leads to nonuniform treatment and difficulty in effectively reaching sidewalls [23–25]. Surface dielectric barrier discharges (SDBD) are a promising approach in this context, as they can produce plasma that propagates along dielectric surfaces and generates reactive species directly at the plasma-treated material interface [26,27].

https://doi.org/10.3390/plasma9030037

In the present work, we investigate a surface dielectric barrier discharge generated from liquid electrodes and propagated along the inner surface of dielectric tubes. In this configuration, plasma filaments travel along the tube wall and interact directly with the treated surface while the tube is gradually filled with water acting as a counter electrode [27–29]. This process leads to simultaneous exposure of microorganisms to direct plasma effects and to plasma-activated liquid formed in situ, which combines gas-phase reactive species, short-lived radicals, and long-lived reactive compounds dissolved in the liquid phase [30]. To the best of our knowledge, such a configuration, in which plasma propagates along the treated material while plasma-activated water is continuously generated, has not been investigated for biofilm removal from the internal surfaces of hollow objects. Understanding the interplay between these processes is important for developing plasma technologies suitable for decontamination of confined geometries, such as tubes and catheters.

2. Materials and Methods

2.1. Surface Dielectric Barrier Discharge Plasma Treatment Setup

Figure 1 presents a visual representation of the reactor configuration, including a schematic of the reactor assembly and a photograph of the generated plasma discharge. The discharge was operated in ambient air at atmospheric pressure. The power to the liquid electrodes was supplied by a high-voltage resonance generator (Lifetech-300W, Brno, Czech Republic) coupled with a function generator (FY3200S-24M, Zhengzhou, China). The electrical characteristics of the discharge were monitored with a digital oscilloscope (Tektronix TBS 2104; 100 MHz; 1 GSa/s, Shanghai, China) connected to a voltage (Tektronix P6015A, Shanghai, China) and current (Pearson Electronics 4100, Palo Alto, CA, USA) probe. The high-voltage sine waveform was generated at frequencies in the range of 26–37 kHz, with the voltage adjusted according to the required discharge power. Although the generator is capable of producing voltages up to 20 kV, the maximum voltage applied under the experimental conditions of this study was approximately 13 kV peak-to-peak, corresponding to a discharge power of 15 W. The Lissajous figure method, displaying the applied voltage and the transferred charge, was used to calculate the discharge power. The standard deviation of the measured power was up to a maximum of 0.5 W. An additional capacitor (10 nF) was added to the circuit to perform these measurements.

Because the liquid level inside the tube changes during treatment, the electrical characteristics of the discharge may vary slightly with the position of the gas–liquid interface. Therefore, prior to the experiments, the discharge power was determined at different liquid levels using the Lissajous method. During treatment, the excitation frequency was adjusted within the resonant frequency range to maintain maximum power transfer and keep the discharge power close to the selected operating value. More details on the electrical characteristics of this SDBD configuration can be found in [31].

For the ignition of the plasma inside the tube, a polytetrafluoroethylene (PTFE) tube, obtained from TB EPOX s.r.o. (Czech Republic), was used. The tube's outer and inner diameters were 9 mm and 8 mm, respectively. The experimental setup involved a glass vessel with a volume of 250 mL, filled with a conductive liquid (oxalic acid solution with a conductivity of 8 mS/cm). Oxalic acid solution was selected as the liquid electrode because it provides the conductivity required for stable SDBD operation while avoiding some of the disadvantages observed with inorganic electrolytes. During treatment with salt-containing solutions, evaporation of water can lead to salt crystallization on the polymer surface. Such deposits can locally distort the electric field, attract plasma filaments, and result in localized energy deposition and potential damage to the polymer. Oxalic acid was therefore used as a practical electrolyte for the present reactor configuration, based on our

previous development of this discharge system. The PTFE tube was immersed in this solution. Subsequently, the tube was gradually filled with the treated solution (sterilized tap water with a conductivity of 390 ± 37 μS cm^{-1} and a pH of 7.9), which did not mix with the oxalic acid solution. The liquid was introduced into the tube using a syringe pump, allowing precise control of the flow rate with increments of 0.1 mL/min. Both the liquid in the vessel and in the tube were connected to the generator via stainless-steel electrodes.

To facilitate handling, the treated PTFE tubes were cut into lengths of 10–13 cm. The total treated length of the tube that was treated during the experiments was approximately 5 cm from the middle of the tube. However, it should be mentioned that the proposed treatment principle is not inherently limited to this length. The process can be extended to longer tubes by appropriate modifications of the reactor configuration, while maintaining the same treatment concept.

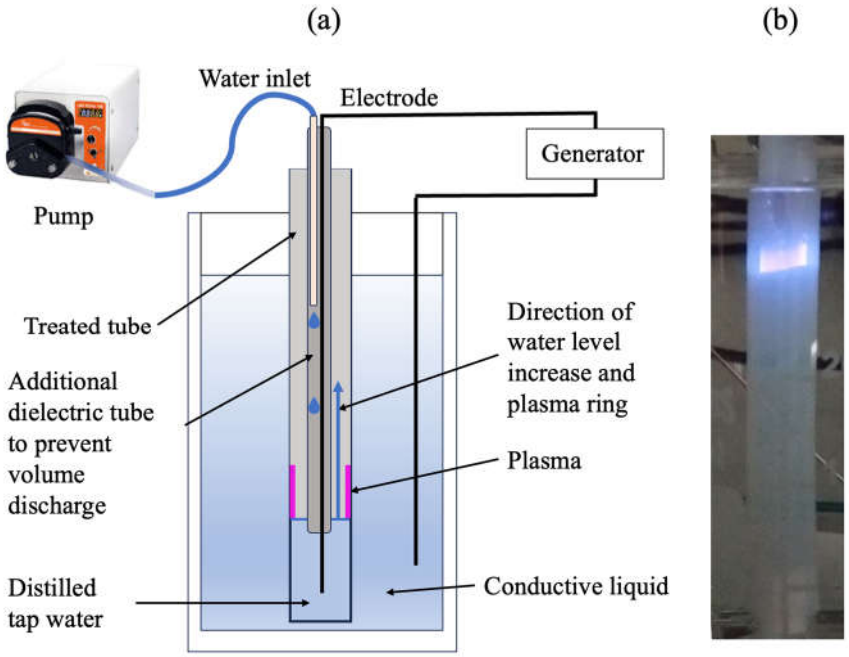

Figure 1. Schematic setup used for the SDBD plasma discharge ignition inside the dielectric tube (**a**), photo of the SDBD inside the dielectric tube (**b**).

2.2. Physicochemical Characterization of Plasma-Activated Water

The discharge interacting with water solutions facilitates an effective transfer of plasma-generated gaseous reactive species. By using UV–VIS absorption spectroscopy (*Shimadzu UV-1800, Kyoto, Japan*), the main aqueous species, such as hydrogen peroxide H_2O_2, nitrite NO_2^-, and nitrate NO_3^- were detected, and their absolute concentrations were evaluated. The presented results are the average of at least five measured samples.

The detection of dissolved ozone was performed by the indigo blue assay. It is a simple, quantitative, colorimetric, and standardized method for ozone detection in water and wastewater [32]. In acidic conditions, O_3 rapidly decolorizes the indigo potassium trisulfonate dye, and the colourless product isatin is formed by the bleaching process. The decrease in absorbance at 600 nm (ε = 2.38 × 104 M^{-1} cm^{-1}) is linear with the increasing concentration of the dissolved O_3. However, it should be noted that this method may not be perfectly specific enough for O_3. It was previously shown that it may cross-correlate, especially with ·OH radicals or other ROS in the PAW [33]. Therefore, the indigo blue assay that was used to detect $O_{3(aq)}$ might have overestimated the real $O_{3(aq)}$ concentration.

The concentration of H_2O_2 was evaluated by the titanium oxysulfate ($TiOSO_4$) assay under acidic conditions [34]. The reaction of titanyl ions Ti^{4+} with H_2O_2 leads to the formation of a yellow-colored complex of pertitanic acid H_2TiO_4 with an absorption maximum at 407 nm. The color intensity is proportional to the H_2O_2 concentration. To prevent H_2O_2 decomposition via reaction with NO_2^- under acidic conditions, after discharge treatment, the sample was immediately stabilized with a 60 mM sodium azide NaN_3 solution. Sodium azide reduces NO_2^- into molecular N_2 and preserves H_2O_2 concentration intact [6]. The used volume ratio of sample: NaN_3: $TiOSO_4$ was 10:1:5.

Concentrations of NO_2^- were evaluated by using Griess reagents under acidic conditions [35,36] using the chemicals and according to the protocol (Cayman Chemicals Nitrate/Nitrite Colorimetric Assay Kit # 780001, Ann Arbor, MI, USA). This method is easy to perform and has been approved as precise for NO_x^- measurement in the PAW produced by plasma discharge [33]. The reaction of nitrites (NO_2^-) with the Griess reagents yields a deep purple azo compound with an absorption maximum of 540 nm.

The total NO_x^- concentration was evaluated by using 10 mM 2,6-xylenol and an acid mixture (H_2SO_4:H_3PO_4 as 1:1) as the reagent. The 10 mM xylenol mixture was prepared by adding 122.16 mg 2,6-xylenol to 100 mL of 10% glacial acetic acid. The used volume ratio of sample: acid: xylenol was 1:8:1. The absorption maximum was recorded between 290 nm and 350 nm after subtracting the control in this region. The maximum peak is directly proportional to the concentration of NO_x^-. If the concentration of NO_x^- was too high, we diluted the sample with deionized water to adjust the NO_x^- concentration in the linear absorbance range. Finally, the NO_3^- concentration was obtained by subtracting the previously measured NO_2^- concentration from the NO_x^- concentration [36].

The ranges of the calibration curves and the respective R^2 values, according to which the RONS determination in liquids was performed, are:

- H_2O_2: 50–2000 μM, $R^2 = 0.9996$
- NO_2^-: 2–50 μM, $R^2 = 0.9995$
- NO_x^-: 100–1000 μM, $R^2 = 0.9914$
- O_3 is calculated based on the absorbance difference.

In case when the concentrations of the RONS were out of these calibration ranges, the samples were diluted to fit the range.

2.3. Bacterial Strain and Culture Conditions

Escherichia coli has been identified as a common biofilm former in chronic wounds and has thus been selected for this study. *E. coli* CCM 3954 was routinely maintained on Luria–Bertani (LB) agar and cultured in liquid LB medium at 37 °C.

2.4. Plasma Treatment of Planktonic E. coli

An overnight culture of *E. coli* was diluted 100-fold in fresh growth medium prior to the plasma treatment. Subsequently, 1 mL of the diluted bacterial suspension was transferred into a sealed (from the bottom) dielectric tube and exposed to the plasma under various operating conditions (discharge power and treatment duration). Immediately after plasma exposure, the treated suspensions were serially diluted in sterile water. Aliquots of the appropriate dilutions were plated onto nutrient agar plates and incubated under standard conditions. After exposure, the number of colony-forming units (CFU) was determined, and bacterial concentration was expressed in CFU/mL.

2.5. Viability Measurement of Planktonic E. coli by Flow Cytometry

To evaluate the cell membrane integrity and recovery potential of planktonic *E. coli* after the direct plasma treatment and treatment with PAW, propidium iodide (PI) staining

was used. PI is a DNA-binding dye that penetrates cells with compromised membranes [37].

Following the plasma treatment, the bacterial suspension was divided into two equal aliquots to evaluate recovery under different conditions. The first aliquot remained in the original suspension, while the second was transferred into nutrient-rich LB medium. Cell viability was monitored at specific time intervals (0, 30, 60, and 120 min after treatment) using PI staining at a final concentration of 2.4 µM. PI-positive cells were detected using a Cytoflex S flow cytometer (Beckman Coulter, Krefeld, Germany) with a blue laser (488 nm) and PE channel (585/42). The data were analyzed with CytExpert 2.4 software (Beckman Coulter, Inc., Krefeld, Germany, 2011–2019).

2.6. Plasma Treatment and Analysis of Biofilms

2.6.1. Preparation of Biofilm Samples

PTFE tubes used in this study were first washed with tap water, thoroughly rinsed with deionized water, and dried. The tubes were then wrapped in aluminum foil and sterilized by autoclaving. Sterile tubes were subsequently filled with *E. coli* suspension at an initial concentration of approximately 10^8 CFU/mL to allow bacterial adhesion (positive control). Adhesion was performed under static conditions at 37 °C for 4 h. After this period, non-adherent planktonic cells were aspirated, and the tubes were gently rinsed with sterile physiological saline. Negative control samples were prepared by incubating sterile tubes in sterile LB medium under similar conditions. Following the adhesion step, the tubes were placed into sterile 50 mL Falcon tubes, filled with sterile LB medium, and incubated at 37 °C for 48 h to allow biofilm formation. This incubation period represents a commonly used laboratory model for *E. coli* biofilm development.

2.6.2. Biofilm Removal Experiments

The effect of PAW on established biofilms was evaluated by introducing freshly prepared PAW into the polymer tubes containing the previously formed biofilm rinsed with sterile tap water to remove planktonic cells. The volume of PAW was not strictly controlled; however, a sufficient volume was used to ensure complete coverage of the investigated biofilm-containing surface. For direct plasma treatment, the rinsed biofilm-containing tubes were subjected to the SDBD plasma under the defined experimental conditions.

Following either PAW or direct plasma treatment, the tubes were transferred into a known volume of sterile physiological saline. Bacterial cells were detached from the inner tube surface by vortexing followed by ultrasonication for 10 min to ensure effective recovery of bacterial cells. The suspensions obtained were serially diluted, and aliquots (20 µL) were plated onto agar plates. The plates were incubated at 37 °C for 24 h, after which the colonies were enumerated to determine the bacterial concentration. The $\log_{10}$ reduction was calculated by comparing the bacterial counts of treated samples with those of the corresponding untreated controls.

2.6.3. Crystal Violet Staining of Biofilms

The presence of biofilms on the inner surface of the tubes was verified visually using crystal violet staining. After removing the planktonic cells by rinsing with physiological saline, biofilms were fixed by adding methanol to the inner surfaces of the tubes and incubating for 15 min at room temperature. Methanol was then allowed to evaporate completely. Subsequently, 0.1% (*w*/*v*) crystal violet solution was added to the tubes and incubated for 30 min at room temperature. The excess stain was then removed by gently washing the tubes under running tap water, and the stained tubes were allowed to dry for visualization.

2.7. Statistical Analysis

Assays were performed in at least three independent experiments, and data were expressed as means ± standard deviation. Basic statistical analysis of data, such as calculating means and standard deviation, was conducted using Microsoft Office Excel 2016 functions. Significance was calculated by one-way analysis of variance (ANOVA) followed by Tukey's multiple comparison test in the GraphPad Prism 6.00 software (GraphPad Software Inc., San Diego, CA, USA). A p-value of <0.05 was considered statistically significant.

In flow cytometry measurements, the statistical significance between control and plasma-treated samples at individual time points was evaluated using a paired two-tailed t-test at * $p \leq 0.05$; ** $p \leq 0.01$; *** $p \leq 0.001$.

3. Results and Discussion

3.1. Physicochemical Characterization of the SDBD System

3.1.1. Electrical and Optical Characteristics of the Plasma Discharge

The plasma generated by the SDBD exhibits a filamentary structure, composed of many microdischarges that travel along the inner walls of the polymer tubes. High-speed imaging has shown that these microdischarges are extremely short-lived, lasting less than 10 ns. Despite their transient nature, the combined effects of the self-induced airflow [38], and the high repetition rate of the microdischarges (26–37 kHz) cause the plasma to appear visually diffuse and nearly homogeneous [29].

Observations of the plasma ring under different power levels have shown that increasing the applied power from 5 W to 15 W led to both an increase in the plasma-covered area and a higher filament density, creating a more intense yet stable treatment environment. At lower powers, individual filaments extended roughly 3 mm along the polymer surface, whereas at 15 W, the filament lengths increased to approximately 7 mm.

For a comprehensive analysis of the discharge's electrical and optical characteristics, including optical emission spectroscopy, ICCD imaging, and detailed electrical measurements, readers are referred to our previous publications [29,39,40].

3.1.2. Formation and Evolution of Reactive Species in PAW

The antimicrobial efficacy of the plasma system is determined by the nature, concentration, and stability of the reactive species generated during discharge operation. In the present SDBD configuration, the interaction of the plasma with the liquid enhances the formation of both short-lived radicals (•OH, O_2•$^-$, O, NO) and long-lived reactive species (H_2O_2, NO_2^-, NO_3^-). Therefore, the effectiveness of the SDBD system was first characterized by measuring RONS generation and the associated physicochemical changes in the treated liquid.

During SDBD operation in ambient air, energetic electrons initiate gas-phase dissociation and excitation reactions, resulting in the formation of atomic oxygen (O), hydroxyl radicals (•OH), nitrogen oxides (NO, NO_2), and ozone (O_3). At the plasma–liquid interface, these species dissolve into the liquid, where secondary reactions play an important role in their stability and conversion. These species are well-documented antimicrobial agents that affect bacterial membranes, cause oxidative stress, and damage cellular components [8,41,42]. The balance between reactions in the plasma and secondary reactions in the liquid determines the final composition of the PAW solution and, consequently, its antimicrobial activity. In the present configuration, the SDBD with liquid electrodes provides a favorable environment for the formation of both oxygen- and nitrogen-based RONS [31]. Consequently, the concentration of these species in the treated liquid is an indirect indicator of plasma chemistry and antimicrobial activity.

Figure 2 shows the concentration of RONS in the liquid inside the polymer tube used as one of the electrodes during treatment times ranging from 30 to 180 s. During plasma treatment of liquid, at the lower applied power, H_2O_2 exhibited a pronounced increase over time, reaching a maximum concentration of ~1450 μM at 3 min. NO_3^- concentrations also increased steadily, peaking at ~1500 μM, whereas NO_2^- concentrations remained low, consistent with the rapid conversion of NO_2^- to NO_3^-. The concentration of dissolved O_3 was found to be negligible, indicating its fast degradation and/or consumption in secondary reactions. The generation of O_3 and NO_2 in the gaseous phase, which can dissolve in water, was also observed in our earlier studies of similar discharges [30]. The $O_{3(aq)}$ concentration was found to be stable at approximately 5 μM in this reactor configuration. The concentration of NO_2^- increased with specific energy input up to approximately 800 J/mL, after which it slightly decreased.

When the applied power was increased to 15 W, the RONS concentrations in water increased significantly. Even after 30 s of operation, the H_2O_2 reached 700 μM, and in 180 s, ~2900 μM. As in the previous case, the concentrations of H_2O_2 and NO_3^- increased with time. Similarly, the NO_2^- peaked in 45 s of treatment. After that, it was not detected in the treated liquid.

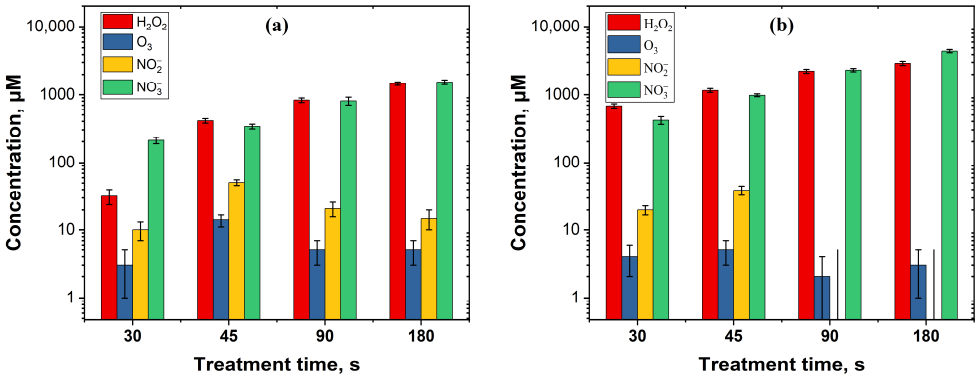

Figure 2. Concentrations of RONS generated in the PAW at 5 W (**a**) and 15 W (**b**).

Increasing treatment duration and discharge power resulted in progressively higher H_2O_2 concentrations, reaching the millimolar range under the most intensive conditions. The progressive accumulation of H_2O_2 is mainly attributed to recombination reactions of hydroxyl radicals leading to H_2O_2 in the gas phase, followed by its dissolution into the liquid or directly within the plasma-affected aqueous layer [43]:

$$\cdot OH + \cdot OH + M \rightarrow H_2O_2 + M \quad (1)$$

H_2O_2 can also be formed by a liquid phase reaction from dissolved HO_2 radicals [44].

$$\cdot HO_2 + \cdot HO_2 \rightarrow H_2O_2 + O_2 \quad (2)$$

or by a sequence of e and H^+ associative reactions (3) and (4):

$$\cdot HO_2 + e^- \rightarrow HO_2^- \quad (3)$$

$$HO_2^- + H^+ \rightarrow H_2O_2 \quad (4)$$

Hydrogen peroxide is relatively stable in aqueous solution and therefore acts as a long-lived reservoir of oxidants. Although its inherent oxidation potential is lower than that of the •OH radical, it can decompose to generate highly reactive hydroxyl radicals that induce oxidative stress in the treated solution.

In contrast, the behavior of reactive nitrogen species in this system differs from many air plasma configurations reported in the literature. While NO_2^- is typically considered an

important intermediate species, in the present discharge configuration, only minimal steady-state concentrations were detected.

The high oxidative potential of the SDBD plasma can explain the negligible accumulation of NO_2^- [33,43,44]:

$$NO_2^- + O_3 \rightarrow NO_3^- + O_2 \quad (5)$$

Additionally, the formation of nitrite and nitrate ions in the liquid phase involves complex chemistry that is strongly dependent on pH conditions. A significant decrease in pH was observed with increasing treatment intensity (Figure 3), and the primary reactions that take place are acidic disproportionation of $NO_{2(aq)}^-$ to $NO_{3(aq)}^-$ [6,31]

$$3NO_2^- + 2H^+ \rightarrow 2NO + NO_3^- + H_2O \quad (6)$$

The temporary formation of peroxynitrous acid (ONOOH), which is usually formed through the combination of H_2O_2 and NO_2^- in acidic environments, is possible. However, peroxynitrous acid is very unstable and immediately decomposes into •OH and $•NO_2$ radicals or NO_3^- [6,31,43].

$$H_2O_2 + NO_2^- + H^+ \rightarrow ONOOH + H_2O \quad (7)$$

$$ONOOH \rightarrow NO_3^- + H^+ \quad (8)$$

$$ONOOH \rightarrow \cdot OH + \cdot NO_2 \quad (9)$$

Consequently, nitrate becomes the dominant and stable nitrogen species in the treated water, while nitrite acts primarily as a transient intermediate. The steady accumulation of NO_3^- therefore reflects the high oxidative capacity of the discharge rather than a limitation in nitrogen chemistry. Although nitrate itself is relatively unreactive, its formation is accompanied by the generation of nitric acid, leading to a measurable decrease in pH (Figure 3).

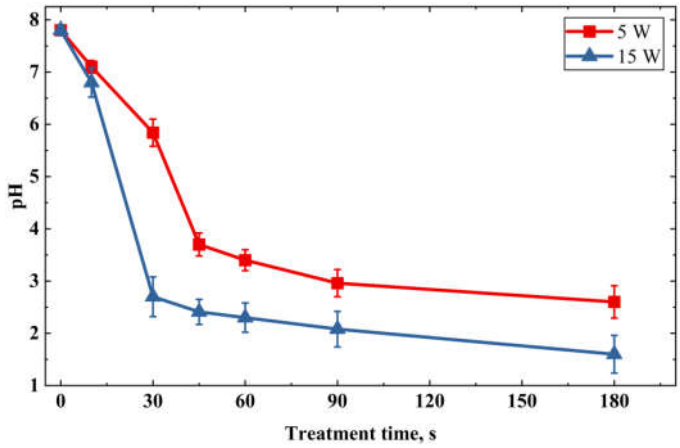

Figure 3. Dependence of the PAW pH on the plasma treatment time.

3.1.3. Temperature Effects

Thermal effects may be another mechanism that contributes to the reduction in the bacterial cell number. To eliminate this possibility, the treatment time of the water was limited to 3 min per 1 mL of sample. At the maximum power of 15 W, the temperature of the tap water after treatment was only 32 °C. This moderate temperature rise is insufficient to cause significant thermal reduction in the bacterial cell number.

Another important factor to consider is the temperature of the plasma itself. In a previous study using the same plasma configuration [45], optical emission spectroscopy

(OES) was used to estimate the rotational temperature of a similar discharge. The measured rotational temperature was approximately 330 K, which is generally considered a good approximation of the gas temperature in atmospheric pressure plasmas. This relatively low temperature indicates that the discharge operates in a non-thermal regime.

To experimentally visualize the spatial and temporal distribution of this thermal load across the polymeric material, real-time infrared (IR) thermography was conducted using an infrared camera. Due to geometric constraints, optical reflections, and line-of-sight limitations within the tube, the measurements were performed with the plasma ignited on the outer surface of the tube. This configuration provides an excellent thermodynamic approximation of the material internal treatment.

Representative infrared camera images are shown in Figure 4. Figure 4a,b were recorded after 10 s of plasma operation and illustrate the temperature distribution associated with the active discharge. To evaluate the maximum thermal load that could be imposed on the material, Figure 4c presents the temperature distribution measured after 1 min of plasma exposure while the plasma ring remained stationary. Under normal operating conditions, the plasma source continuously moves along the tube, resulting in significantly shorter local exposure times. Therefore, the stationary configuration shown in Figure 4c can be considered a worst-case scenario with respect to thermal loading.

The infrared images demonstrate that plasma treatment results only in moderate surface heating of the PTFE tube. Although localized temperature increases may occur in regions directly exposed to plasma filaments, the overall thermal load remains relatively low. These observations, together with the previously reported rotational temperature measurements, indicate that heat-related effects are unlikely to contribute significantly to the observed biofilm removal or reduction in the bacterial cell number under the applied treatment conditions.

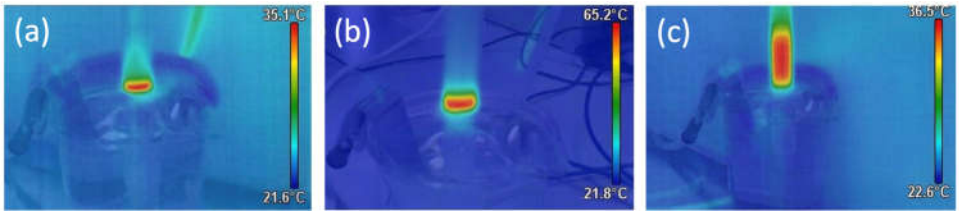

Figure 4. Infrared camera images: applied power 5 W (**a**), applied power 15 W (**b**), and temperature load on the PTFE tube after plasma treatment for 1 min at one spot (**c**).

3.2. Antimicrobial Activity Against Planktonic Bacteria

3.2.1. Antibacterial Performance of PAW Generated by Surface DBD

The antibacterial activity of the plasma-activated water produced by the surface dielectric barrier discharge was evaluated by monitoring the survival of *E. coli* as a function of the plasma treatment conditions. In the control group, the bacterial population remained constant without any decrease in population size, maintaining a constant value of 7.5 $\log_{10}$ CFU/mL for the entire time of exposure, confirming that the observed reduction in the culturable bacteria was solely due to plasma-induced effects.

Effect of Plasma Treatment Power and Duration

Figure 5 illustrates the bacterial population dynamics, expressed as $\log_{10}$ CFU/mL, during exposure to PAW treated for various durations and at two discharge powers (5 and 15 W). The exposure time ranged from 0 to 360 min.

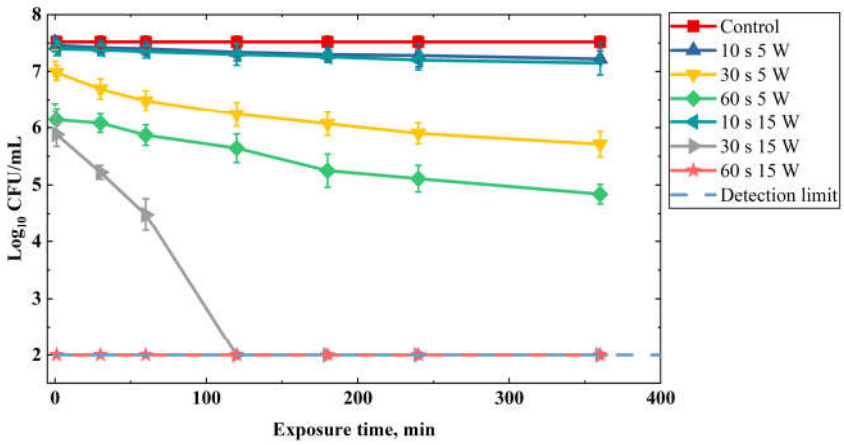

Figure 5. *E. coli* population levels after exposure to PAW treated for 10 s up to 1 min, at 5 and 15 W power.

Limited antibacterial activity was seen immediately after mixing PAW with the bacterial suspension. PAW generated with a treatment duration of 10 s did not produce a measurable reduction in bacterial counts. The only statistically significant antibacterial activity was seen when the PAW was prepared with treatment times of 60 s at 5 W, giving a bacterial count of 6.3 $\log_{10}$ CFU/mL, and at 15 W for treatment times of 30 s and 60 s, giving bacterial counts of 6.1 $\log_{10}$ CFU/mL and 6.0 $\log_{10}$ CFU/mL, respectively.

At a discharge power of 5 W, when the treatment time was extended to 10, 30, and 60 s, bacterial counts declined gradually over 360 min, with final counts of approximately 7.2, 5.7, and 4.8 $\log_{10}$ CFU/mL, respectively. When the PAW was treated for 10 s, the bacterial population was reduced to approximately 7.1 $\log_{10}$ CFU/mL after 6 h. However, when the PAW was treated for 30 s, the bacterial population was immediately reduced by approximately 1.5 $\log_{10}$ CFU/mL and then decreased rapidly over the subsequent exposure period. Within 120 min, the bacterial population was reduced below the detection level (~2 $\log_{10}$ CFU/mL). The PAW treated for 1 min exhibited the strongest antibacterial effect and total reduction in the bacterial population immediately after mixing with the *E. coli* suspension.

Although agar plate cultivation results indicated that PAW generated by 15 W plasma for 1 min had the strongest antimicrobial effect, flow cytometry analysis (Figure 6) showed only a low percentage of PI-positive cells. Furthermore, the proportion of PI-positive cells decreased over time, from 10% immediately after treatment to 1.6% after 120 min exposure, although this trend was not statistically significant.

This apparent discrepancy between the culturability assessed by agar plate cultivation and the viability estimated by flow cytometry may arise because propidium iodide staining reflects membrane permeability rather than irreversible cell death. Plasma treatment can transiently permeabilize bacterial membranes, allowing PI to enter cells that may subsequently recover membrane integrity and survive [46,47]. In addition, the observed decrease in the proportion of PI-positive cells during post-treatment exposure may not solely reflect the recovery of membrane integrity. Severely damaged cells may undergo progressive disintegration or shrinkage following the treatment, eventually becoming undetectable by flow cytometry. At the same time, plasma-induced oxidative stress

can trigger a viable but non-culturable (VBNC) state, in which cells remain metabolically active but lose the ability to form colonies on agar plates [48].

Intracellular RONS may induce oxidative DNA damage, including oxidized bases and DNA strand breaks. In bacteria, such damage activates the "SOS" response, leading to cell cycle arrest and prioritizing DNA repair over cell division [49,50]. As a result, cells may survive but temporarily fail to proliferate on cultivation media.

Interestingly, when cells were transferred into nutrient-rich LB medium, the percentage of PI-positive cells increased to 25% after 30 min of exposure in LB and subsequently decreased to 3.6% after 120 min of exposure (Figure 6). Similarly to the trend observed in PAW-incubated cells, this decrease was not statistically significant. Nevertheless, the transient increase in PI-positive cells observed during the early exposure period may indicate that the sudden restoration of metabolic activity in nutrient-rich conditions initially exacerbated oxidative stress in sublethally damaged cells. Subsequently, surviving cells may have recovered and restored membrane integrity [51–53]. In addition, VBNC cells are known to exhibit enhanced resistance to oxidative stress through activation of antioxidative stress response pathways [54].

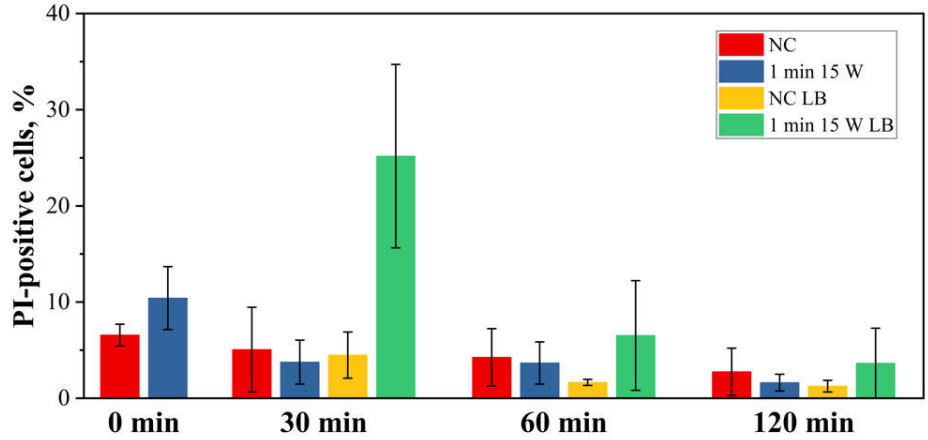

Figure 6. Percentage of dead (PI-positive) cells in planktonic culture determined by flow cytometry following plasma-activated water (PAW) treatment. NC—non-treated control incubated in water; NC LB—non-treated control incubated in nutrient-rich LB medium; 1 min 15 W—PAW-treated sample; 1 min 15 W LB—PAW treated sample subsequently incubated in nutrient-rich LB medium. Time points (0, 30, 60 and 120 min) represent exposure times in PAW after treatment. Statistical significance between control and plasma-treated samples at individual time points was evaluated using a paired two-tailed *t*-test. No statistically significant differences were observed at any time point.

Persistence of Reactive Species and Oxidative Inactivation Mechanism

The continued decrease in bacterial concentrations after treatment and during the exposure period further supports the fact that PAW exhibits antimicrobial efficacy, attributable to long-lived oxidizing species. Similar post-treatment effects have been reported for plasma-treated liquids and surfaces, in which hydrogen peroxide and nitrates maintain antimicrobial activity for extended periods [55,56].

Hydrogen peroxide plays a central role in this process. As demonstrated in Section 3.1, millimolar H_2O_2 concentrations accumulate in PAW under higher energy input. H_2O_2 can diffuse across bacterial membranes and induce intracellular oxidative stress. Although H_2O_2 is less reactive compared to the highly oxidative •OH, the compound can decompose into •OH again, both spontaneously and catalytically, thereby causing oxidative damage [57]. This mechanism explains the progressive inactivation observed at lower

discharge power (5 W), where oxidative stress accumulates over time rather than causing immediate cell death.

At higher discharge power (15 W), the concentration of H_2O_2 and associated reactive species exceeds the threshold required for rapid membrane peroxidation and intracellular redox imbalance. Consequently, oxidative damage is instantaneous, resulting in immediate or near-immediate reduction in the target bacteria cells number. The strong correlation between RONS concentrations (Section 3.1, Figure 2) and bacterial $\log_{10}$ reduction (Figure 5) confirms that oxidative stress represents the dominant antibacterial pathway in SDBD-generated PAW.

An additional control experiment was performed to evaluate the effect of H_2O_2 on *E. coli*. The bacteria were exposed to a 1 mM H_2O_2 solution prepared in distilled water. The $\log_{10}$ reduction in culturable bacterial cell number was 1.12 immediately after mixing and increased to 1.69 after 180 min of exposure. These reductions were less pronounced than those obtained using PAW prepared for 60 s at both investigated power levels. This result indicates that H_2O_2 alone cannot account for the antibacterial activity of PAW under the investigated conditions. Other plasma-generated species and physicochemical effects therefore likely contribute to the observed reduction in bacterial cell number and may substantially influence the overall treatment efficacy.

Acidification of the solution during plasma treatment is an additional factor that improves antimicrobial activity. It is well known that acidification is an effective method to increase the reactivity of RONS. It has been shown that acidification improves the penetration of hydrogen peroxide into bacterial membranes [58]. However, acidification alone does not reproduce the observed bactericidal effects. To evaluate the effect of acidification on bacterial survival, an additional control experiment was performed using sulfuric acid (H_2SO_4) solutions prepared in distilled water at pH values of 5, 3, and 2. The bacteria were exposed to these solutions under otherwise comparable conditions. The corresponding $\log_{10}$ reductions in bacterial cell numbers were 1.04, 1.05, and 1.08, respectively, indicating that acidification alone, even at pH 2, produced only a limited reduction under the conditions investigated. Several studies have shown a similar effect that artificially acidified solutions lacking plasma-generated RONS do not achieve comparable inactivation [59,60]. Thus, it is suggested that acidification acts synergistically with plasma-generated oxidants rather than serving as the primary lethal factor. The low level of NO_2^- accumulation observed in this system suggests that peroxynitrite ($ONOO^-$) formation (Equation (7)) is not a dominant mechanism, unlike in other studies [12,61]. Instead, bacterial inactivation is primarily driven by hydrogen peroxide and derived oxidative species. These findings are in good agreement with previous reports that highlighted the significance of H_2O_2 and •OH radicals in the plasma-activated media [57,62].

3.2.2. Antibacterial Performance of Direct Plasma Treatment

Effect of Discharge Power and Treatment Duration

Similarly to previous experiments, the bacterial inactivation kinetics following direct plasma exposure were evaluated by measuring *E. coli* populations ($\log_{10}$ CFU/mL) as a function of exposure time after direct SDBD treatment at two discharge powers (5 W and 15 W). Figure 7 presents the evolution of bacterial counts over 0–360 min of exposure for three treatment durations (10, 30, and 60 s), alongside a non-treated control. The untreated control showed a slight increase in bacterial concentration during exposure.

For the 5 W treatments, it was found that the 10 s treatment had a negligible effect during the exposure period, yielding ~1 $\log_{10}$ reduction, whereas the 30 s treatment resulted in a steady decline over the exposure period. However, even after 360 min, a small fraction of bacteria remained viable (~3 $\log_{10}$ reduction). Increasing the treatment duration to 1 min showed a marked improvement in inactivation efficiency. Evidently, after 120

min, no surviving colonies were detected. Treatments at 15 W for 10 s were more effective in terms of their impact on the bacteria than those at 5 W. A ~2 $\log_{10}$ reduction was achieved after 360 min of exposure. Longer treatment times led to significantly greater and more rapid reduction in bacterial cell numbers. The treatment at 15 W for 30 s resulted in approximately a 1 $\log_{10}$ reduction in bacterial counts immediately after treatment, with the bacteria becoming undetectable after a short exposure period. The 1 min treatment at 15 W completely inactivated bacteria, with no detectable bacteria present throughout the exposure period.

These results demonstrate a clear energy-dependent enhancement of bactericidal efficiency. Compared to PAW treatment, direct plasma exposure results in faster and more complete reduction in bacterial cell numbers under the same power and duration.

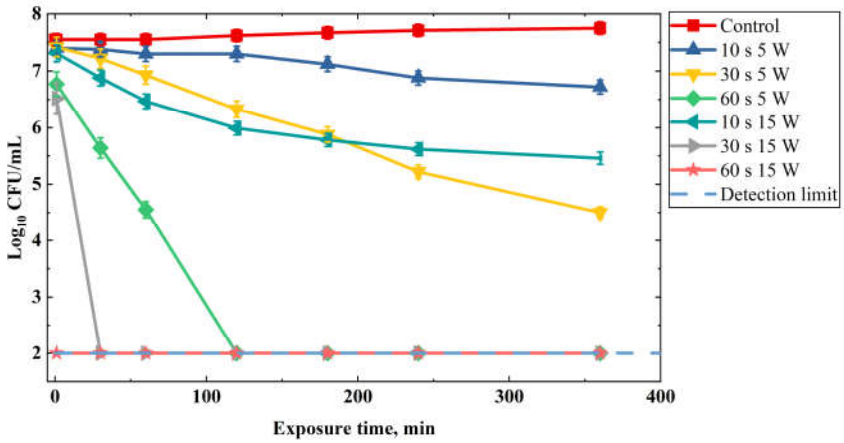

Figure 7. *E. coli* population in relation to the exposure time after direct plasma treatment inside the tube.

Similarly to the PAW experiments, flow cytometry analysis following direct plasma treatment revealed a discrepancy between membrane integrity assessed by propidium iodide staining and culturability determined by agar plate cultivation. However, direct plasma exposure was substantially more effective than PAW, resulting in approximately 80% PI-positive cells immediately after treatment. During the subsequent two-hour exposure, the proportion of PI-positive cells gradually decreased to 27.4% (Figure 8).

As discussed for PAW-treated cells, this trend may reflect partial restoration of membrane integrity in surviving cells, resulting in a lower proportion of cells permeable to propidium iodide. However, direct plasma treatment can also cause extensive damage to the cell envelope through the combined action of reactive species, UV radiation, electric fields, and charged particles. Consequently, some severely damaged cells may undergo progressive shrinkage, fragmentation, or disintegration during post-treatment exposure and therefore become undetectable by flow cytometry, further contributing to the observed decrease in PI-positive cells. At the same time, plasma-induced oxidative stress may trigger a possible VBNC state, in which cells remain metabolically active but lose the ability to form colonies on agar plates [63]. Furthermore, transfer into nutrient-rich LB medium resulted in an even higher proportion of PI-positive cells (78% after 30 min of exposure), supporting the hypothesis that restoration of metabolic activity can aggravate oxidative stress in sublethally damaged cells [52,53]. Together, these findings suggest that although the underlying mechanisms are similar to those observed after PAW treatment, the additional physical and chemical stressors associated with direct plasma exposure lead to more extensive cellular damage.

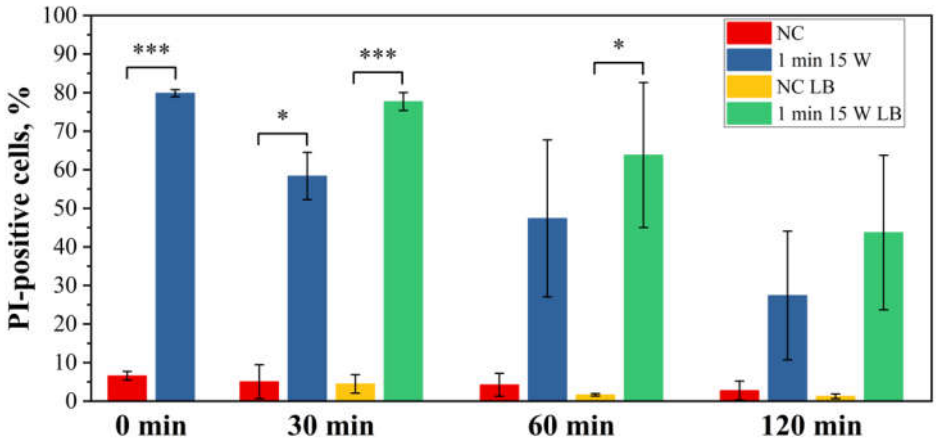

Figure 8. Percentage of dead (PI-positive) cells in planktonic culture determined by flow cytometry following direct plasma treatment. NC—non-treated control incubated in water; NC LB—non-treated control incubated in nutrient-rich LB medium; 1 min 15 W—plasma-treated sample; 1 min 15 W LB—plasma treated sample subsequently incubated in nutrient-rich LB medium. Time points (0, 30, 60, 120 min) represent exposure times after treatment. Statistical significance between control and plasma-treated samples at individual time points was evaluated using a paired two-tailed *t*-test at * $p \leq 0.05$; *** $p \leq 0.001$.

Mechanisms of Direct Plasma Inactivation

The superior efficacy of direct plasma treatment can be explained by the simultaneous interaction of chemical and physical factors at the plasma–liquid–cell interface. In contrast to PAW, where long-lived species dominate, direct exposure delivers short-lived radicals and electrophysical effects directly to the bacterial cell surface [64,65]. Although short-lived reactive species may contribute to the enhanced efficacy of direct plasma treatment, their concentrations and fluxes were not quantitatively determined in the present study. Therefore, their contribution is discussed as a possible mechanism based on the observed results and available literature rather than as an experimentally confirmed explanation. Also, though the present results demonstrate the overall effectiveness of the direct plasma treatment, the individual contributions of these factors were not experimentally quantified, as it was beyond the scope of the present study. Their potential influence on the observed antibacterial effect is nevertheless discussed below in the context of previously reported findings in the literature.

Short-lived reactive species, including atomic oxygen (O), hydroxyl radicals (•OH), singlet oxygen ($^1O_2$), and excited species, play a decisive role in oxidative damage. These species exhibit extremely high oxidation potentials and can penetrate the thin liquid boundary layer surrounding bacterial cells, initiating lipid peroxidation and protein oxidation [41,42]. The penetration of atomic oxygen into a treated liquid has been demonstrated in several studies, which show a strong correlation with inactivation efficiency in bacterial membranes [13]. Under atmospheric pressure conditions, reactive oxygen species are widely considered the dominant contributors to microbial inactivation [13].

Although some UV radiation is produced during DBD discharge, its role in microbial inactivation is considered secondary. UV-C can cause localized DNA damage [66], but the effectiveness of UV-C at atmospheric pressure is strongly restricted by absorption in the surrounding gases [13,66]. Thus, the role of plasma-produced UV is of secondary importance in the inactivation of microorganisms in air-operated plasma systems.

In the present study, UV radiation is also unlikely to have significantly influenced bacterial activity during the plasma treatment because this type of radiation was not present in sufficient intensities to account for the observed results. Optical emission

spectroscopy measurements performed on a similar discharge type revealed that emission components below 300 nm were absent [29]. OES measurements were also taken in the current discharge configuration, and although the results were similar to those mentioned, the spectrum exhibited a considerably higher noise level, which made the interpretation difficult (not presented). Therefore, the reduction in bacterial cell numbers observed here is more likely attributed to reactive oxygen and nitrogen species, charged particles, and other plasma-induced chemical processes.

In addition to chemical oxidation, direct plasma treatment exposes microorganisms to transient electric fields and to charge accumulation on their surfaces. Electrostatic stress can induce membrane depolarization and electroporation, resulting in leakage of intracellular contents and irreversible damage [67,68]. This mechanism is often compared with pulsed electric field treatment, in which membrane perforation leads to the loss of viability [69].

However, in the present configuration, the electric field responsible for these electrophysical effects is not expected to be uniformly distributed throughout the entire discharge volume. In SDBD, the electric field is typically strongly localized near the dielectric surface and at the exposed electrode edges, where the field strength is maximal. As a result, the intensity of the electric field decreases rapidly with increasing distance from the dielectric interface, leading to a strongly heterogeneous field distribution within the plasma region [70].

This localization of the electric field is closely related to the generation of transient microdischarge filaments that are characteristic of DBD discharges. In general, plasma filaments are initiated in the discharge volume at points where the strength of the local electric field is above the breakdown value. Once initiated, they propagate along the dielectric interface, depositing surface charge that dynamically modifies the local electric field distribution and influences subsequent filament formation [71]. This self-regulating behavior contributes to the filamentary and highly localized nature of the discharge.

Experimental observations further support this description. Spectroscopic measurements and modeling study have shown that both emission intensity and electric field magnitude are the highest near the powered electrode and decay with distance from the discharge region [72]. Moreover, numerical simulations indicate that the dielectric properties of the material play a crucial role in shaping the electric field distribution and controlling filament propagation. Together, these findings confirm that in SDBD systems, electrophysical effects are predominantly confined to regions close to the plasma–surface interface, which has important implications for localized plasma–biofilm interactions.

Consequently, in the configuration used in this work, the strongest electrophysical interactions with microorganisms are expected to occur primarily in the near-tube region where the plasma is in direct contact with the water. At the same time, the fast decay of the electric field with distance from the dielectric surface suggests that the liquid is subjected to significantly weaker electrophysical effects. In contrast, the chemically reactive species produced in the plasma can still penetrate the surrounding liquid.

Electron microscopy studies have reported plasma-induced morphological alterations in *E. coli*, including cell deformation, cytoplasmic damage, membrane disruption, and leakage of intracellular contents under some treatment conditions [41,67]. However, in our study, flow-cytometric analysis did not reveal a comparably pronounced loss of membrane integrity, despite a marked reduction in culturability. This suggests that, under our experimental conditions, plasma-induced reduction in bacterial cell numbers may have been driven predominantly by sublethal oxidative and intracellular damage rather than immediate large-scale membrane permeabilization. Thus, direct plasma treatment combines long-lived oxidative chemistry with highly reactive, short-lived species and

electrophysical effects, accounting for the accelerated inactivation kinetics with respect to PAW treatment alone.

3.3. Antimicrobial Activity Against Biofilms

Biofilms are a microbial phenotype that is far more resistant than planktonic cells because of the extracellular matrix, the metabolic state of the cells, and the difficulty of antimicrobial penetration. To evaluate the suitability of the SDBD system for surface decontamination applications, established bacterial biofilms were grown on the inner surfaces of polymer tubes and were subsequently exposed directly to plasma generated within the same tube.

3.3.1. Antibiofilm Performance of PAW

Effect of the Discharge Power and Treatment Duration

Figure 9 illustrates the survival of biofilm cells after plasma treatment at different discharge powers and exposure times. The viable counts were measured after the PAW treatment and subsequent exposure. The results show that PAW exhibited limited antimicrobial activity against biofilms after 5 min of exposure. The highest antimicrobial activity of PAW was observed when it was generated for 3 min, resulting in approximately a 1.3 $\log_{10}$ reduction in viable bacterial cell numbers. PAW generated for shorter treatment durations had limited effects on the viability of biofilm-associated bacterial cells. The reduction in the viability of biofilm-associated bacterial cells may be due to the antimicrobial activity of PAW, which contains RONS accumulated in the liquid during plasma treatment. Longer plasma treatment increased RONS concentration in PAW, thereby increasing oxidative stress on the biofilm and leading to the observed reduction in biofilm viability.

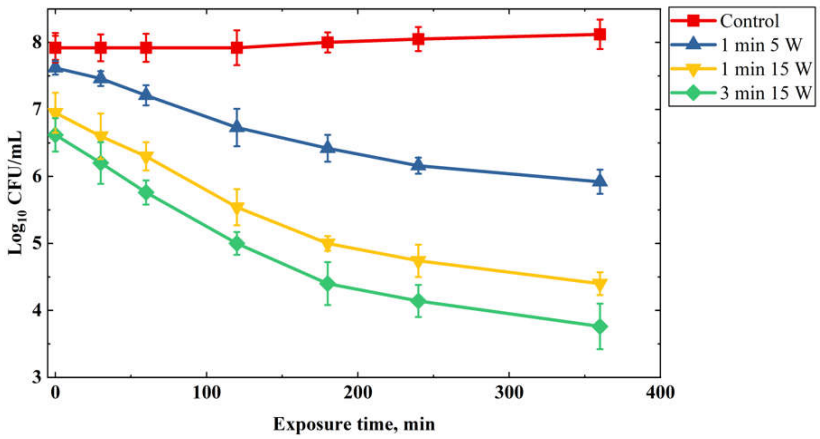

Figure 9. Survival of biofilm cells after exposure to plasma-activated water generated at different treatment times and discharge powers, followed by different exposure scenarios.

Following the PAW treatment and exposure, the survival kinetics of the bacterial population differed significantly between the control and PAW-treated cultures (Figure 9). The control culture maintained high cell numbers, with only a minor change from ~8 to ~8.1 $\log_{10}$ CFU/mL over 360 min. In contrast, all PAW treatments produced time-dependent reductions in colony counts, and the extent of reduction depended strongly on the PAW generation conditions (i.e., discharge power and duration).

The reduction in the bacterial cell numbers was moderate when the PAW treatment was applied at 5 W for 1 min, with the viable count reduced to ~6 $\log_{10}$ CFU/mL after 360 min. A greater reduction in the viable cell count was observed when the treatment was

carried out at 15 W for 1 min, resulting in a viable cell count of ~4.4 $\log_{10}$ CFU/mL after 360 min. The greatest reduction in the bacterial cell numbers was observed when the PAW treatment was performed at 15 W for 3 min, with the viable cell count dropping below 3.8 $\log_{10}$ CFU/mL after 360 min.

Thus, increasing plasma power and treatment time significantly improved the antibiofilm efficacy. The strongest treatment performed notably better than the weaker ones, as expected, demonstrating an energy-dependent cell number reduction pattern similar to that observed in planktonic cultures discussed in Section 3.2. However, it is important to note that more energy is required to inactivate biofilms to the same extent as planktonic bacteria, indicating their greater resistance to antimicrobial treatments.

Mechanisms of Biofilm Inactivation by PAW

The enhanced resistance of biofilms is often associated with the structural protection offered by the EPS network surrounding the biofilm-associated microorganisms. The EPS network restricts the penetration of reactive species into the biofilm interior and can even react with oxidants before they reach the embedded microorganisms. In addition, components of the EPS can actively interact with and neutralize oxidizing agents, thereby reducing their availability for direct attack on bacterial cells.

Despite this protective function, the present study indicates that sufficiently strong oxidative conditions can progressively compromise the biofilm's structural integrity. Prolonged plasma activation of water led to increased concentrations of RONS, which correlated with measurable reductions in biofilm viability. These observations suggest that the antimicrobial action of PAW involves an initial interaction with the EPS matrix, followed by enhanced penetration of reactive species and subsequent damage to the underlying bacterial cells. Similar mechanisms have been reported in previous studies investigating the interaction of plasma-activated liquids with biofilm systems [42,73].

The inactivation process can be described as a sequence of oxidative events. Initially, reactive species target extracellular components such as polysaccharides and proteins, thereby weakening the biofilm's structural stability. As the matrix progressively degrades, its permeability increases, allowing deeper diffusion of reactive species into previously protected regions. This facilitates direct interaction with bacterial cells, leading to oxidative damage of cell membranes and intracellular structures. The accumulation of long-lived species, particularly hydrogen peroxide at millimolar concentrations, together with plasma-induced acidification, appears to play a key role in sustaining this process. Ultimately, this combined chemical action results in the effective disruption of the biofilm and the loss of bacterial viability.

3.3.2. Antibiofilm Performance of SDBD

Effect of the Discharge Power and Treatment Duration

Finally, to evaluate the plasma's ability to remove biofilms directly, biofilms formed on the inner surface of the polymer tube were subjected to the SDBD generated within the tube. In contrast to the PAW-based biofilm treatments discussed in the previous section, in which antimicrobial action depended solely on the long-lived reactive species in PAW, the biofilm in this configuration interacted directly with the plasma formed within the dielectric tube. At the same time, the tube was gradually filled with water, serving as the counter electrode of the discharge and thus becoming progressively plasma-activated during the treatment. Thus, the treatment can be viewed as a dynamic plasma–liquid process, in which plasma filaments sweep along the biofilm surface while reactive species simultaneously accumulate in the rising liquid surface.

Figure 10 shows the antimicrobial efficiency of the SDBD system applied to *E. coli* biofilms grown on the inner surface of a polymer tube. The results are reported as

reductions in viable bacterial numbers relative to a control sample immersed in water for 10 min without plasma exposure, thereby accounting for any possible effects of hydration or mechanical removal of the biofilm from the surface during the treatment procedure.

No significant decrease in bacterial cell numbers was observed in the control samples, validating the assumption that immersion in water does not remove biofilms. In contrast, plasma exposure led to a clear decrease in viable bacterial populations, demonstrating the antibiofilm activity of the SDBD system. The reduction in the number of biofilm-associated bacterial cells increased markedly with increasing discharge power and treatment duration. Shorter exposure times (up to approximately 15 s) produced only partial reductions in viable cell numbers, reaching up to 2 $\log_{10}$ reduction at 5 W and up to 5 $\log_{10}$ reduction at 15 W. With increasing treatment time, the reduction in biofilm-associated bacterial cell numbers increased substantially, reaching approximately 3.8 $\log_{10}$ at 5 W, while no viable bacteria were detected following treatment at 15 W.

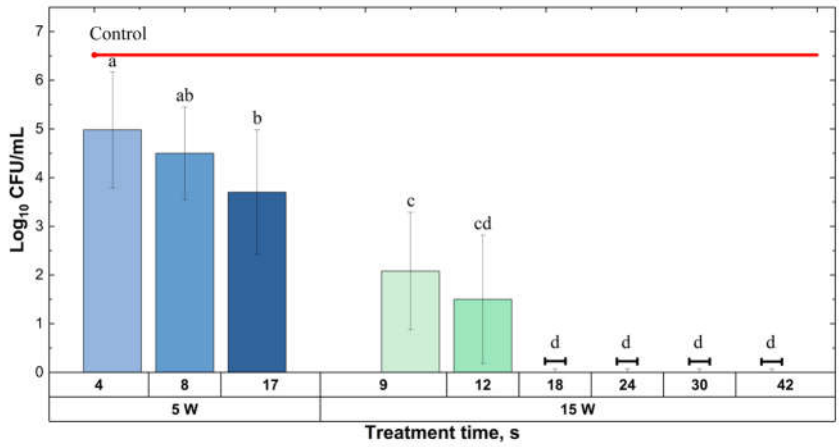

Figure 10. Log_{10} reduction in *E. coli* biofilms inside a 5 cm polymer tube after plasma treatment for different treatment times and applied powers.

It should be noted that in the present study, the shortest direct plasma treatment time was 9 s. This is due to the discharge configuration and the operating conditions of the experimental setup. The output power of the HV generator sustaining the SDBD is strongly dependent on the system resonance frequency. The resonance frequency of the system in the experiments varies with the level of the liquid in the tube reactor, as the electrical properties of the plasma-liquid system depend on the electrode geometry and the dielectric properties.

Due to the relatively small internal volume of the tubes used to form biofilms, even slight changes in the liquid level resulted in corresponding changes in the resonant frequency. Under these conditions, stable operation of the SDBD could only be achieved by continuously adjusting the generator frequency. Since the frequency control was performed manually, a short delay inevitably occurred between the optimal resonance condition and the corresponding adjustment of the generator settings.

To ensure a stable discharge operation and homogeneous plasma exposure of the biofilm surface, it was therefore necessary to limit the rate of liquid level change during the treatment process. This condition, together with the characteristic length of plasma filaments along the tube surface, determined the minimum treatment time that could be reliably applied under the experimental conditions. The relatively lower efficiency observed at the shortest treatment times may also be associated with the transient stabilization of the discharge during the initial phase of the plasma ignition. Although the plasma appeared visually homogeneous, the fast changes in the liquid level and the presence of water droplets on the tube surface might cause slight movement of the active plasma

region along the inner wall of the tube. Under such conditions, not all areas of the biofilm surface were exposed uniformly during the shortest treatment periods.

As the treatment time increased, the plasma region became more stable, and its motion slowed, allowing the discharge to interact with all surfaces of the biofilm and resulting in more homogeneous treatment. The simultaneous intensification of both mechanisms can explain the higher antibacterial efficiency observed at increased discharge power. Stronger plasma conditions produce higher gas-phase radical densities and more energetic filament-biofilm interactions, while also increasing the rate of reactive species transfer into the liquid phase. Together, these effects lead to faster disruption of the biofilm matrix and greater bacterial inactivation.

Based on the previous flow cytometry results, only one treatment duration was selected for further analysis from this set of samples. As demonstrated in Figure 10, a 30 s plasma treatment resulted in complete biofilm inactivation as determined by conventional cultivation methods. However, flow cytometric analysis performed after treatment revealed a substantially lower proportion of PI-positive cells, reaching only approximately 20% (Figure 11). This discrepancy between culturability assessed by agar plate cultivation and membrane integrity assessed by flow cytometry suggests that a considerable fraction of biofilm cells remained membrane-intact but were no longer capable of forming colonies, indicating severe sublethal injury or a transition into the possible VBNC state [48].

Following the treatment, the proportion of PI-positive cells increased during the first 30 and 60 min of exposure (Figure 11). This trend suggests that plasma-induced damage continued to manifest after the end of the treatment, potentially as a consequence of intracellular oxidative stress, progressive loss of membrane integrity, and secondary damage processes [3,20,74]. Unlike planktonic cells, in which the proportion of PI-positive cells decreased during post-treatment exposure (Figure 8), biofilm cells exhibited a delayed increase in membrane permeability, indicating a distinct cellular response to plasma-induced stress.

Upon transfer to LB medium, a lower proportion of PI-positive cells was generally observed compared with water-incubated samples, except at the 120 min time point. This behavior differs from the planktonic cells (Figure 8), where exposure in LB resulted in a higher proportion of PI-positive cells than exposure in water. These observations suggest that the effects of post-treatment metabolic activation differ between planktonic and biofilm-associated cells, possibly reflecting the distinct physiological state and stress tolerance mechanisms of biofilm populations [75,76].

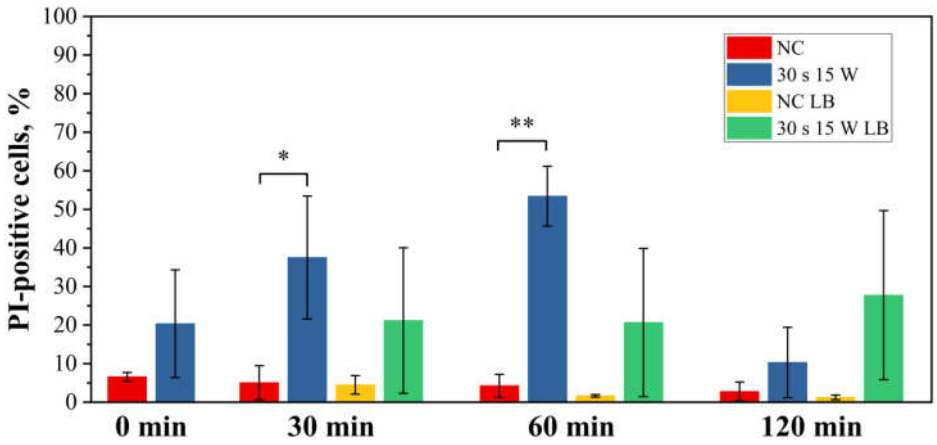

Figure 11. Percentage of dead (PI-positive) cells in biofilm determined by flow cytometry following direct plasma treatment. NC—non-treated control incubated in water; NC LB—non-treated control incubated in nutrient-rich LB medium; 24 s and 30 s 15 W—plasma treated sample; 24 s and 30 s 15 W LB—plasma treated sample subsequently incubated in nutrient-rich LB medium. Time points (0,

30, 60, 120 min) represent exposure times after treatment. Statistical significance between control and plasma-treated samples at individual time points was evaluated using a paired two-tailed *t*-test at * $p \leq 0.05$; ** $p \leq 0.01$.

Visual Proof of the SDBD Performance

Figure 12 presents representative images documenting the individual stages of the treatment procedure and demonstrating the effects of the SDBD plasma treatment on PTFE tube surfaces. The untreated PTFE tube shown in Figure 12a exhibits the original appearance of the material prior to any plasma exposure or biological contamination. This sample serves as the baseline control representing a pristine, uncolonized polymer surface completely free of organic contaminants. After plasma treatment at 15 W for 18 s (Figure 12b) and subsequent crystal violet staining, slight changes in the surface appearance can be observed. The tube exhibits a very faint, homogeneous violet tint. This may be associated with plasma-induced surface modification. Such modifications are commonly attributed to the interaction of plasma with the polymer surface, leading to changes in surface chemistry, wettability, and surface energy [77,78].

Figure 12c shows the PTFE tube after biofilm formation stained with crystal violet. A visible layer of deposited biomass can be observed on the inner surface of the tube, indicating successful biofilm establishment before the plasma removal experiments.

Following plasma treatment, the tube shown in Figure 12d demonstrates the complete eradication of the dark purple staining and the recovery of a very faint violet baseline (virtually identical to the clean, plasma-treated control tube (Figure 12b) providing direct visual proof of the outstanding cleaning and stripping performance of the SDBD discharge.

Although the visual assessment alone does not provide quantitative information on the degree of microbial inactivation or biofilm removal efficiency, the images presented serve as qualitative evidence of the SDBD system's ability to interact with and remove biologically contaminated layers from PTFE surfaces. These observations are consistent with previously reported plasma-assisted biofilm removal results.

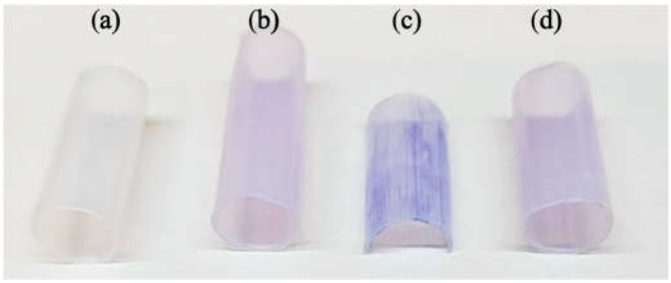

Figure 12. Image of the original PTFE tube (**a**), plasma-treated tube (**b**), tube with deposited biofilm (**c**), and tube after plasma biofilm removal experiment (**d**).

Mechanisms of Biofilm Removal by the SDBD System

Contrary to the PAW treatments in Section 3.3.1, where only the long-lived plasma species dissolved in the solution contributed to the antimicrobial activity, the present configuration exposes the biofilm to propagating plasma filaments that interact directly with the biofilm surface. These transient microdischarges generate high local concentrations of short-lived reactive species such as hydroxyl radicals, atomic oxygen, and excited oxygen species. Such species may cause rapid oxidative damage to the bacterial membranes and EPS, contributing to the destabilization of the biofilm structure.

In addition to purely chemical effects, direct plasma treatment introduces a range of electrophysical mechanisms that can further contribute to microbial inactivation.

Energetic electrons and ions interacting with the biofilm surface can induce localized charge accumulation and transient electric fields. As discussed in the previous section, transient electric fields and charge accumulation can induce electrophysical stress on microbial cells, leading to membrane depolarization and electroporation effects. In the current SDBD configuration, these effects are expected to occur predominantly within the localized plasma filaments, where the electric field strength and charged-particle density reach their highest values. This spatial localization of electric fields is therefore consistent with the experimentally observed behavior of microbial inactivation. Furthermore, the interaction of the plasma filaments with the biofilm surface may lead to a rise in the temperature of the biofilm, promoting further destabilization of the biofilm matrix. Although thermal effects are not a major contributor to the SDBD system's antimicrobial action, they may support the overall biofilm removal process.

At the same time, the gradual filling of the tube with water results in the continuous formation of plasma-activated water during the treatment process. As the liquid interacts with the plasma discharge, RONS dissolve into the liquid and accumulate over time, forming long-lived oxidants such as hydrogen peroxide. These species can diffuse into the biofilm matrix and contribute to antimicrobial activity even in regions that are not in immediate contact with the plasma filaments. Consequently, the biofilm is subjected to a combined plasma–liquid treatment environment, in which direct plasma effects dominate at the plasma–surface interface, while dissolved reactive species provide additional chemical oxidation within the liquid. This combined effect is likely to enhance the efficiency of the biofilm removal process.

4. Conclusions

In this study, the antibacterial performance of a surface dielectric barrier discharge system with liquid electrodes was investigated with the main aim of evaluating its suitability for plasma-assisted decontamination of internal tubular surfaces contaminated with *E. coli* biofilms. From a physical point of view, this configuration can be regarded as a moving plasma–biofilm interaction zone, where the plasma filaments move along the internal surface of the tube while the liquid electrode gradually fills the tube volume. Such a configuration promotes intense interaction between plasma microdischarges and the tube surface covered with biofilm, enabling localized delivery of reactive species and enhancing the overall plasma-assisted decontamination process.

The SDBD plasma generated reactive oxygen and nitrogen species in water, which resulted in the formation of plasma-activated water characterized by the accumulation of hydrogen peroxide (up to 3 mM) and nitrate ions (up to 4.5 mM)and a significant reduction in pH. Although the nitrite formation was minimal in the present system, its rapid oxidation to nitrate indicates efficient conversion of nitrogen oxides within the plasma–liquid system. From the experiments, it was proven that these chemical conditions are responsible for the antimicrobial properties of PAW.

The antimicrobial effect of PAW on the planktonic cells of *E. coli* was strongly dependent on the plasma operating conditions. Higher discharge power and longer treatment duration led to higher concentrations of reactive species and enhanced antibacterial efficacy. Total inactivation of bacteria was achieved after exposure to PAW prepared by 15 W plasma treatment for 1 min. The reduction in planktonic *E. coli* cell numbers continued during the exposure period, indicating the long-lasting effect of reactive species generated in the liquid. The results of flow cytometry measurements demonstrate that plasma-induced cell number reduction is largely associated with oxidative stress-mediated sublethal injury rather than direct membrane disruption. The persistence of membrane integrity despite the loss of culturability indicates a transition of a significant fraction of cells into the possible VBNC state.

https://doi.org/10.3390/plasma9030037

The direct plasma treatment demonstrated even greater antimicrobial efficiency, especially on biofilms formed on the inner surfaces of polymer tubes. The biofilm was exposed simultaneously to plasma filaments, gas-phase reactive species, and reactive species formed in the liquid. This dynamic plasma–liquid interaction created a combined chemical and physical treatment environment that enhanced biofilm disruption. Biofilm inactivation was strongly enhanced by increasing the discharge power and the treatment time, with complete reduction in viable bacterial cell numbers achieved under the most intense treatment conditions used in this study. Compared to planktonic bacteria, biofilms exhibited higher resistance to plasma exposure, which can be attributed to the protective structure of the extracellular polymeric substance matrix. Nevertheless, the combined effects of reactive species, localized electric fields, and direct plasma–surface interaction were able to overcome this protection and allow for effective biofilm inactivation and removal.

Overall, the findings demonstrate that the investigated SDBD plasma configuration can generate chemically active plasma environments and thus achieve efficient reduction in bacterial cell numbers both in liquid media and on material surfaces. The ability to generate plasma directly inside tubular geometries and to simultaneously produce plasma-activated liquid makes this system particularly promising for plasma-assisted cleaning and decontamination of confined surfaces and internal channels, where conventional chemical treatments may be less effective.

Author Contributions: Conceptualization, O.G. and Z.M.; methodology, O.G. and B.G.K.; validation, O.G. and B.G.K.; formal analysis, O.G., B.G.K., M.P. and S.R.; investigation, O.G., B.G.K., M.P. and S.R.; data curation, O.G., M.P. and S.R.; writing—original draft preparation, O.G. and M.P.; writing—review and editing, O.G., B.G.K., S.R., M.P., V.V. and Z.M.; visualization, O.G.; supervision, O.G., V.V. and Z.M.; project administration, O.G. and Z.M.; funding acquisition, O.G. All authors have read and agreed to the published version of the manuscript.

Funding: This work was funded by the EU NextGenerationEU through the Recovery and Resilience Plan for Slovakia under the project No. 09I03-03-V04-00094 and by Marie Skłodowska-Curie Action Postdoctoral Fellowship under Horizon Europe with grant agreement number 101066764.

Data Availability Statement: The original contributions presented in this study are included in the article. Further inquiries can be directed to the corresponding author.

Acknowledgments: The authors gratefully acknowledge the CEPLANT Centre for the provision of high-voltage equipment, which significantly contributed to the realization of this research.

Conflicts of Interest: The authors declare no conflicts of interest.

Abbreviations

The following abbreviations are used in this manuscript:

EPS	Extracellular Polymeric Substance
ROS	Reactive Oxygen Species
RONS	Reactive Oxygen and Nitrogen Species
PAW	Plasma Activated Water
DBD	Dielectric Barrier Discharges
SDBD	Surface Dielectric Barrier Discharges
PTFE	Polytetrafluoroethylene
UV	Ultraviolet
LB agar	Luria–Bertani agar
CFU	Colony-Forming Units
PI	Propidium Iodide
ICCD	Intensified Charge-Coupled Device

OES	Optical Emission Spectroscopy
IR	Infrared
VBNC	Viable But Non-Culturable
NC	Non-treated Control
HV	High Voltage

References

1. von Woedtke, T.; Kramer, A.; Weltmann, K.D. Plasma sterilization: What are the conditions to meet this claim? *Plasma Process. Polym.* **2008**, *5*, 534–539. https://doi.org/10.1002/ppap.200800013.
2. Adler, S.; Scherrer, M.; Daschner, F.D. Costs of low-temperature plasma sterilization compared with other sterilization methods. *J. Hosp. Infect.* **1998**, *40*, 125–134. https://doi.org/10.1016/S0195-6701(98)90091-3.
3. Lim, J.; Park, S.; Ryu, S.; Park, S.; Kim, M.S. Different Inactivation Mechanisms of Staphylococcus aureus and *Escherichia coli* in Water by Reactive Oxygen and Nitrogen Species Generated from an Argon Plasma Jet. *Environ. Sci. Technol.* **2025**, *59*, 3276–3285. https://doi.org/10.1021/ACS.EST.4C10363.
4. Rotondo, P.R.; Aceto, D.; Ambrico, M.; Stellacci, A.M.; Faretra, F.; Angelini, R.M.D.M.; Ambrico, P.F. Physicochemical properties of plasma-activated water and associated antimicrobial activity against fungi and bacteria. *Sci. Rep.* **2025**, *15*, 5536. https://doi.org/10.1038/s41598-025-88369-7.
5. Machala, Z.; Tarabová, B.; Sersenová, D.; Janda, M.; Hensel, K. Chemical and antibacterial effects of plasma activated water: Correlation with gaseous and aqueous reactive oxygen and nitrogen species, plasma sources and air flow conditions. *J. Phys. D Appl. Phys.* **2019**, *52*, 034002. https://doi.org/10.1088/1361-6463/aae807.
6. Machala, Z.; Tarabova, B.; Hensel, K.; Spetlikova, E.; Sikurova, L.; Lukes, P. Formation of ROS and RNS in Water Electro-Sprayed through Transient Spark Discharge in Air and their Bactericidal Effects. *Plasma Process. Polym.* **2013**, *10*, 649–659. https://doi.org/10.1002/PPAP.201200113.
7. Weltmann, K.D.; Von Woedtke, T. Plasma medicine—Current state of research and medical application. *Plasma Phys. Control Fusion* **2017**, *59*, 014031. https://doi.org/10.1088/0741-3335/59/1/014031.
8. Guo, H.; Wang, Y.; Wang, J.; Tang, S.; Wang, T. Review on application of non-thermal plasma for disinfection: Direct plasma and indirect plasma-activated water. *Chin. Chem. Lett.* **2026**, *37*, 111275. https://doi.org/10.1016/J.CCLET.2025.111275.
9. Xu, Y.; Bassi, A. Non-thermal plasma decontamination of microbes: A state of the art. *Biotechnol. Prog.* **2025**, *41*, e3511. https://doi.org/10.1002/btpr.3511.
10. Hertwig, C.; Reineke, K.; Ehlbeck, J.; Knorr, D.; Schlüter, O. Decontamination of whole black pepper using different cold atmospheric pressure plasma applications. *Food Control* **2015**, *55*, 221–229. https://doi.org/10.1016/j.foodcont.2015.03.003.
11. Ehlbeck, J.; Schnabel, U.; Polak, M.; Winter, J.; Von Woedtke, T.; Brandenburg, R.; von dem Hagen, T.; Weltmann, K.-D. Low temperature atmospheric pressure plasma sources for microbial decontamination. *J. Phys. D Appl. Phys.* **2011**, *44*, 013002. https://doi.org/10.1088/0022-3727/44/1/013002.
12. Lukes, P.; Dolezalova, E.; Sisrova, I.; Clupek, M. Aqueous-phase chemistry and bactericidal effects from an air discharge plasma in contact with water: Evidence for the formation of peroxynitrite through a pseudo-second-order post-discharge reaction of H_2O_2 and HNO_2. *Plasma Sources Sci. Technol.* **2014**, *23*, 015019. https://doi.org/10.1088/0963-0252/23/1/015019.
13. Lu, X.; Ye, T.; Cao, Y.; Sun, Z.; Xiong, Q.; Tang, Z.; Xiong, Z.; Hu, J.; Jiang, Z.; Pan, Y. The roles of the various plasma agents in the inactivation of bacteria. *J. Appl. Phys.* **2008**, *104*, 053309. https://doi.org/10.1063/1.2977674.
14. Qian, J.; Yan, W.; Sheng, X.; Zhao, L.; Zhang, J.; Wang, J.; Raghavan, V. Mechanism of action of plasma-activated water on biomacromolecules in Salmonella Enteritidis: Biological effect, computer simulation, and transcriptomics-based analysis. *Chem. Eng. J.* **2024**, *496*, 153946. https://doi.org/10.1016/j.cej.2024.153946.
15. Mai-Prochnow, A.; Zhou, R.; Zhang, T.; Ostrikov, K.; Mugunthan, S.; Rice, S.A.; Cullen, P.J. Interactions of plasma-activated water with biofilms: Inactivation, dispersal effects and mechanisms of action. *npj Biofilms Microbiomes* **2021**, *7*, 11. https://doi.org/10.1038/s41522-020-00180-6.
16. Vleugels, M.; Shama, G.; Deng, X.T.; Greenacre, E.; Brocklehurst, T.; Kong, M. Atmospheric plasma inactivation of biofilm-forming bacteria for food safety control. *IEEE Trans. Plasma Sci.* **2005**, *33*, 824–828. https://doi.org/10.1109/TPS.2005.844524.
17. Flynn, P.B.; Gilmore, B.F. Understanding plasma biofilm interactions for controlling infection and virulence. *J. Phys. D Appl. Phys.* **2018**, *51*, 263001. https://doi.org/10.1088/1361-6463/AAC475.
18. Gilmore, B.F.; Flynn, P.B.; O'Brien, S.; Hickok, N.; Freeman, T.; Bourke, P. Cold Plasmas for Biofilm Control: Opportunities and Challenges. *Trends Biotechnol.* **2018**, *36*, 627–638. https://doi.org/10.1016/j.tibtech.2018.03.007.

19. Lavrikova, A.; Janda, M.; Bujdáková, H.; Hensel, K. Eradication of single- and mixed-species biofilms of P. aeruginosa and S. aureus by pulsed streamer corona discharge cold atmospheric plasma. *Sci. Total Environ.* **2025**, *959*, 178184. https://doi.org/10.1016/J.SCITOTENV.2024.178184.
20. Maybin, J.A.; Thompson, T.P.; Flynn, P.B.; Skvortsov, T.; Hickok, N.J.; Freeman, T.A.; Gilmore, B.F. Cold atmospheric pressure plasma-antibiotic synergy in Pseudomonas aeruginosa biofilms is mediated via oxidative stress response. *Biofilm* **2023**, *5*, 100122. https://doi.org/10.1016/J.BIOFLM.2023.100122.
21. Kovalóvá, Z.; Zahoran, M.; Zahoranová, A.; Machala, Z. Streptococci biofilm decontamination on teeth by low-temperature air plasma of dc corona discharges. *J. Phys. D Appl. Phys.* **2014**, *47*, 224014. https://doi.org/10.1088/0022-3727/47/22/224014.
22. Kovalova, Z.; Leroy, M.; Jacobs, C.; Kirkpatrick, M.J.; Machala, Z.; Lopes, F.; O Laux, C.; DuBow, M.S.; Odic, E. Atmospheric pressure argon surface discharges propagated in long tubes: Physical characterization and application to bio-decontamination. *J. Phys. D Appl. Phys.* **2015**, *48*, 464003. https://doi.org/10.1088/0022-3727/48/46/464003.
23. Wu, S.; Guo, Y.; Ouyang, F.; Zhou, B.; Hu, B.; Cheng, H. Characteristics of the plasma sheath in helium discharge within dielectric tubes. *Plasma Sci. Technol.* **2023**, *25*, 045402. https://doi.org/10.1088/2058-6272/ac9e93.
24. Balazs, D.J.; Triandafillu, K.; Chevolot, Y.; Aronsson, B.; Harms, H.; Descouts, P.; Mathieu, H.J. Surface modification of PVC endotracheal tubes by oxygen glow discharge to reduce bacterial adhesion. *Surf. Interface Anal.* **2003**, *35*, 301–309. https://doi.org/10.1002/sia.1533.
25. Glukhoy, Y.; Kerzhner, T.; Ryaboy, A. Rf Antenna Assembly for Treatment of Inner Surfaces of Tubes with Inductively Coupled Plasma. U.S. Patent 7,967,945, 3 December 2009.
26. Jamali, S.; Kargarian, A. Comparative study of surface modification of fluorinated and non-fluorinated polymers using SDBD air plasma. *Sci. Rep.* **2025**, *15*, 35917. https://doi.org/10.1038/s41598-025-19841-7.
27. Galmiz, O.; Pavliňák, D.; Zemánek, M.; Brablec, A.; Černák, M. Hydrophilization of outer and inner surfaces of Poly(vinyl chloride) tubes using surface dielectric barrier discharges generated in ambient air plasma. *Plasma Process. Polym.* **2017**, *14*, e1600220. https://doi.org/10.1002/ppap.201600220.
28. Galmiz, O.; Zemánek, M.; Pavliňák, D.; Černák, M. Plasma treatment of polyethylene tubes in continuous regime using surface dielectric barrier discharge with water electrodes. *J. Phys. D Appl. Phys.* **2018**, *51*, 195201. https://doi.org/10.1088/1361-6463/aabb49.
29. Galmiz, O.; Pavlinak, D.; Zemanek, M.; Brablec, A.; Černák, M. Study of surface dielectric barrier discharge generated using liquid electrodes in different gases. *J. Phys. D Appl. Phys.* **2016**, *49*, 065201. https://doi.org/10.1088/0022-3727/49/6/065201.
30. Galmiz, O.; Cimerman, R.; Pareek, P.; Janda, M.; Machala, Z. Production of reactive species by using surface dielectric barrier discharge in direct contact with water. *Plasma Sources Sci. Technol.* **2025**, *34*, 025011. https://doi.org/10.1088/1361-6595/adb3cb.
31. Galmiz, O.; Cimerman, R.; Machala, Z. Effect of reactor configuration of surface dielectric barrier discharge in contact with liquids on the production of reactive species. *Chem. Eng. J.* **2026**, *530*, 173630. https://doi.org/10.1016/j.cej.2026.173630.
32. Bader, H.; Hoigné, J. Determination of ozone in water by the indigo method. *Water Res.* **1981**, *15*, 449–456. https://doi.org/10.1016/0043-1354(81)90054-3.
33. Tarabová, B.; Lukeš, P.; Janda, M.; Hensel, K.; Šikurová, L.; Machala, Z. Specificity of detection methods of nitrites and ozone in aqueous solutions activated by air plasma. *Plasma Process. Polym.* **2018**, *15*, 1800030. https://doi.org/10.1002/PPAP.201800030.
34. Eisenberg, G.M. Colorimetric Determination of Hydrogen Peroxide. *Ind. Eng. Chem.-Anal. Ed.* **1943**, *15*, 327–328. https://doi.org/10.1021/I560117A011.
35. Griess, P. Bemerkungen zu der Abhandlung der HH. Weselsky und Benedikt „Ueber einige Azoverbindungen. *Berichte Der Dtsch. Chem. Ges.* **1879**, *12*, 426–428. https://doi.org/10.1002/CBER.187901201117.
36. Moorcroft, M.J.; Davis, J.; Compton, R.G. Detection and determination of nitrate and nitrite: A review. *Talanta* **2001**, *54*, 785–803. https://doi.org/10.1016/S0039-9140(01)00323-X.
37. Rosenberg, M.; Azevedo, N.F.; Ivask, A. Propidium iodide staining underestimates viability of adherent bacterial cells. *Sci. Rep.* **2019**, *9*, 6483. https://doi.org/10.1038/s41598-019-42906-3.
38. Hoskinson, A.R.; Hershkowitz, N. Differences between dielectric barrier discharge plasma actuators with cylindrical and rectangular exposed electrodes. *J. Phys. D Appl. Phys.* **2010**, *43*, 065205. https://doi.org/10.1088/0022-3727/43/6/065205.
39. Cvetanović, N.; Galmiz, O.; Synek, P.; Zemánek, M.; Brablec, A.; Hoder, T. Electron density in surface barrier discharge emerging at argon/water interface: Quantification for streamers and leaders. *Plasma Sources Sci. Technol.* **2018**, *27*, 025002. https://doi.org/10.1088/1361-6595/aaa578.

40. Voráč, J.; Synek, P.; Procházka, V.; Hoder, T. State-by-state emission spectra fitting for non-equilibrium plasmas: OH spectra of surface barrier discharge at argon/water interface. *J. Phys. D Appl. Phys.* **2017**, *50*, 294002. https://doi.org/10.1088/1361-6463/aa7570.
41. Hong, Y.F.; Kang, J.G.; Lee, H.Y.; Uhm, H.; Moon, E.; Park, Y. Sterilization effect of atmospheric plasma on *Escherichia coli* and *Bacillus subtilis* endospores. *Lett. Appl. Microbiol.* **2009**, *48*, 33–37. https://doi.org/10.1111/j.1472-765X.2008.02480.x.
42. Xu, D.; Liu, D.; Wang, B.; Chen, C.; Chen, Z.; Li, D.; Yang, Y.; Chen, H.; Kong, M.G. In Situ OH Generation from O_2^- and H_2O_2 Plays a Critical Role in Plasma-Induced Cell Death. *PLoS ONE* **2015**, *10*, e0128205. https://doi.org/10.1371/journal.pone.0128205.
43. Zhou, R.; Zhou, R.; Prasad, K.; Fang, Z.; Speight, R.; Bazaka, K.; Ostrikov, K. Cold atmospheric plasma activated water as a prospective disinfectant: The crucial role of peroxynitrite. *Green Chem.* **2018**, *20*, 5276–5284. https://doi.org/10.1039/c8gc02800a.
44. Pareek, P.; Kooshki, S.; Toth, P.; Janda, M. Tuning composition of plasma activated water generated by transient spark discharge with electrospray. *Chem. Eng. J.* **2024**, *493*, 152583. https://doi.org/10.1016/j.cej.2024.152583.
45. Pavliňák, D.; Galmiz, O.; Zemánek, M.; Brablec, A.; Čech, J.; Černák, M. Permanent hydrophilization of outer and inner surfaces of polytetrafluoroethylene tubes using ambient air plasma generated by surface dielectric barrier discharges. *Appl. Phys. Lett.* **2014**, *105*, 154102. https://doi.org/10.1063/1.4898134.
46. Barkhade, T.; Nigam, K.; Ravi, G.; Rawat, S.; Nema, S.K. Investigating the effects of microwave plasma on bacterial cell structures, viability, and membrane integrity. *Sci. Rep.* **2025**, *15*, 18052–18072. https://doi.org/10.1038/s41598-025-02312-4.
47. Das, S.; Mohapatra, S.; Kar, S. Elucidating the bacterial inactivation mechanism by argon cold atmospheric pressure plasma jet through spectroscopic and imaging techniques. *J. Appl. Microbiol.* **2024**, *135*, lxae238. https://doi.org/10.1093/JAMBIO/LXAE238.
48. Dolezalova, E.; Lukes, P. Membrane damage and active but nonculturable state in liquid cultures of *Escherichia coli* treated with an atmospheric pressure plasma jet. *Bioelectrochemistry* **2015**, *103*, 7–14. https://doi.org/10.1016/J.BIOELECHEM.2014.08.018.
49. Yost, A.D.; Joshi, S.G. Atmospheric Nonthermal Plasma-Treated PBS Inactivates *Escherichia coli* by Oxidative DNA Damage. *PLoS ONE* **2015**, *10*, e0139903. https://doi.org/10.1371/JOURNAL.PONE.0139903.
50. Gupta, A.; Imlay, J.A. *Escherichia coli* induces DNA repair enzymes to protect itself from low-grade hydrogen peroxide stress. *Mol. Microbiol.* **2022**, *117*, 754–769. https://doi.org/10.1111/MMI.14870.
51. Dodd, C.E.R.; Richards, P.J.; Aldsworth, T.G. Suicide through stress: A bacterial response to sub-lethal injury in the food environment. *Int. J. Food Microbiol.* **2007**, *120*, 46–50. https://doi.org/10.1016/J.IJFOODMICRO.2007.06.008.
52. Hong, Y.; Zeng, J.; Wang, X.; Drlica, K.; Zhao, X. Post-stress bacterial cell death mediated by reactive oxygen species. *Proc. Natl. Acad. Sci. USA* **2019**, *116*, 10064–10071. https://doi.org/10.1073/PNAS.1901730116.
53. Lan, L.; Shi, H. New insights into the formation and recovery of sublethally injured *Escherichia coli* O157:H7 induced by lactic acid. *Food Microbiol.* **2022**, *102*, 103918. https://doi.org/10.1016/J.FM.2021.103918.
54. Liao, X.; Hu, W.; Liu, D.; Ding, T. Stress Resistance and Pathogenicity of Nonthermal-Plasma- Induced Viable-but-Nonculturable Staphylococcus aureus through Energy Suppression, Oxidative Stress Defense, and Immune-Escape Mechanisms. *Appl. Environ. Microbiol.* **2021**, *87*, e02380-20. https://doi.org/10.1128/AEM.02380-20.
55. Darmanin, M.; Fröhling, A.; Bußler, S.; Durek, J.; Neugart, S.; Schreiner, M.; Blundell, R.; Gatt, R.; Schlüter, O.; Valdramidis, V.P. Aqueous and gaseous plasma applications for the treatment of mung bean seeds. *Sci. Rep.* **2021**, *11*, 19681. https://doi.org/10.1038/s41598-021-97823-1.
56. Darmanin, M.; Kozak, D.; de Oliveira Mallia, J.; Blundell, R.; Gatt, R.; Valdramidis, V.P. Generation of plasma functionalized water: Antimicrobial assessment and impact on seed germination. *Food Control* **2020**, *113*, 107168. https://doi.org/10.1016/j.foodcont.2020.107168.
57. Oehmigen, K.; Winter, J.; Hähnel, M.; Wilke, C.; Brandenburg, R.; Weltmann, K.; von Woedtke, T. Estimation of Possible Mechanisms of *Escherichia coli* Inactivation by Plasma Treated Sodium Chloride Solution. *Plasma Process. Polym.* **2011**, *8*, 904–913. https://doi.org/10.1002/PPAP.201000099.
58. Julák, J.; Hujacová, A.; Scholtz, V.; Khun, J.; Holada, K. Contribution to the Chemistry of Plasma-Activated Water. *Plasma Phys. Rep.* **2018**, *44*, 125–136. https://doi.org/10.1134/S1063780X18010075.
59. Ikawa, S.; Kitano, K.; Hamaguchi, S. Effects of pH on bacterial inactivation in aqueous solutions due to low-temperature atmospheric pressure plasma application. *Plasma Process. Polym.* **2010**, *7*, 33–42. https://doi.org/10.1002/ppap.200900090.
60. Oehmigen, K.; Hähnel, M.; Brandenburg, R.; Wilke, C.; Weltmann, K.; von Woedtke, T. The Role of Acidification for Antimicrobial Activity of Atmospheric Pressure Plasma in Liquids. *Plasma Process. Polym.* **2010**, *7*, 250–257. https://doi.org/10.1002/PPAP.200900077.

61. Xu, H.; Wang, J.; Yao, Q.; Dai, X.; Jiao, Z.; Ma, R.; Shao, T. The inactivation mechanism of nitrogen oxides plasma activated water against fungi and the potential risks in forming VBNC state. *Chem. Eng. J.* **2025**, *522*, 167738. https://doi.org/10.1016/J.CEJ.2025.167738.
62. Judée, F.; Simon, S.; Bailly, C.; Dufour, T. Plasma-activation of tap water using DBD for agronomy applications: Identification and quantification of long lifetime chemical species and production/consumption mechanisms. *Water Res.* **2018**, *133*, 47–59. https://doi.org/10.1016/J.WATRES.2017.12.035.
63. Dezest, M.; Bulteau, A.L.; Quinton, D.; Chavatte, L.; Le Bechec, M.; Cambus, J.P.; Arbault, S.; Nègre-Salvayre, A.; Clément, F.; Cousty, S. Oxidative modification and electrochemical inactivation of *Escherichia coli* upon cold atmospheric pressure plasma exposure. *PLoS ONE* **2017**, *12*, e0173618. https://doi.org/10.1371/JOURNAL.PONE.0173618.
64. Tschang, C.Y.T.; Thoma, M. In vitro comparison of direct plasma treatment and plasma activated water on *Escherichia coli* using a surface micro-discharge. *J. Phys. D Appl. Phys.* **2019**, *53*, 055201. https://doi.org/10.1088/1361-6463/AB522A.
65. Los, A.; Ziuzina, D.; Boehm, D.; Cullen, P.J.; Bourke, P. Inactivation Efficacies and Mechanisms of Gas Plasma and Plasma-Activated Water against Aspergillus flavus Spores and Biofilms: A Comparative Study. *Appl. Environ. Microbiol.* **2020**, *86*, e02619-19. https://doi.org/10.1128/AEM.02619-19.
66. Roth, S.; Feichtinger, J.; Hertel, C. Characterization of *Bacillus subtilis* spore inactivation in low-pressure, low-temperature gas plasma sterilization processes. *J. Appl. Microbiol.* **2010**, *108*, 521–531. https://doi.org/10.1111/j.1365-2672.2009.04453.x.
67. Laroussi, M.; Mendis, D.A.; Rosenberg, M. Plasma interaction with microbes. *New J. Phys.* **2003**, *5*, 41. https://doi.org/10.1088/1367-2630/5/1/341.
68. Mendis, D.A.; Rosenberg, M.; Azam, F. A note on the possible electrostatic disruption of bacteria. *IEEE Trans. Plasma Sci.* **2000**, *28*, 1304–1306. https://doi.org/10.1109/27.893321.
69. Mentheour, R.; Machala, Z. Coupled Antibacterial Effects of Plasma-Activated Water and Pulsed Electric Field. *Front Phys.* **2022**, *10*, 895813. https://doi.org/10.3389/fphy.2022.895813.
70. Wang, L.; Wang, Z. Numerical simulation of surface dielectric barrier discharge. In Proceedings of the 2016 IEEE International Conference on Information and Automation, Ningbo, China, 1–3 August 2016; pp. 310–313. https://doi.org/10.1109/ICInfA.2016.7831841.
71. Celestin, S.; Bonaventura, Z.; Guaitella, O.; Rousseau, A.; Bourdon, A. Influence of surface charges on the structure of a dielectric barrier discharge in air at atmospheric pressure: Experiment and modeling. *Eur. Phys. J. Appl. Phys.* **2009**, *47*, 22810. https://doi.org/10.1051/epjap/2009078.
72. Gibalov, V.I.; Pietsch, G.J. The development of dielectric barrier discharges in gas gaps and on surfaces. *J. Phys. D Appl. Phys.* **2000**, *33*, 2618–2636. https://doi.org/10.1088/0022-3727/33/20/315.
73. Mai-Prochnow, A.; Murphy, A.B.; McLean, K.M.; Kong, M.G.; Ostrikov, K. Atmospheric pressure plasmas: Infection control and bacterial responses. *Int. J. Antimicrob. Agents* **2014**, *43*, 508–517. https://doi.org/10.1016/j.ijantimicag.2014.01.025.
74. Lunov, O.; Zablotskii, V.; Churpita, O.; Lunova, M.; Jirsa, M.; Dejneka, A.; Kubinová, Š. Chemically different non-thermal plasmas target distinct cell death pathways. *Sci. Rep.* **2017**, *7*, 600. https://doi.org/10.1038/s41598-017-00689-5.
75. Zhang, Y.; Cai, Y.; Zhang, B.; Zhang, Y.H.P.J. Spatially structured exchange of metabolites enhances bacterial survival and resilience in biofilms. *Nat. Commun.* **2024**, *15*, 7575. https://doi.org/10.1038/S41467-024-51940-3.
76. Mai-Prochnow, A.; Bradbury, M.; Ostrikov, K.; Murphy, A.B. Pseudomonas aeruginosa Biofilm Response and Resistance to Cold Atmospheric Pressure Plasma Is Linked to the Redox-Active Molecule Phenazine. *PLoS ONE* **2015**, *10*, e0130373. https://doi.org/10.1371/JOURNAL.PONE.0130373.
77. Booth, J.P.; Mozetič, M.; Nikiforov, A.; Oehr, C. Foundations of plasma surface functionalization of polymers for industrial and biological applications. *Plasma Sources Sci. Technol.* **2022**, *31*, 103001. https://doi.org/10.1088/1361-6595/ac70f9.
78. Ma, C.; Nikiforov, A.; Hegemann, D.; De Geyter, N.; Morent, R.; Ostrikov, K. Plasma-controlled surface wettability: Recent advances and future applications. *Int. Mater. Rev.* **2023**, *68*, 82–119. https://doi.org/10.1080/09506608.2022.2047420.